Transmission Imaging in Lymphoscintigraphy with a ^{153}Gd Flood Source

Frank P. DiFilippo, Richard C. Brunken, and Donald R. Neumann

Department of Nuclear Medicine, Cleveland Clinic, Cleveland, Ohio

Lymphoscintigraphy uses intradermal or interstitial injections of ^{99m}Tc-labeled tracers to produce images of focal lymph nodes. Because there is little or no anatomic information in the ^{99m}Tc images, a ^{57}Co flood source is sometimes used to provide transmission data along with the emission data. The anatomic shadow from the transmission scan generally improves interpretation and surgical planning. However, the ^{57}Co transmission photons contribute to background on the ^{99m}Tc images, reducing contrast and signal-to-noise ratio (SNR). SNR is related to lesion detection, and some lymph nodes that would be detected in an emission-only scan might not be detected if acquired with a ^{57}Co flood source. An alternative to a ^{57}Co flood source is a ^{153}Gd flood source, which has primary photon emissions well below the ^{99m}Tc emission window, allowing the shadow to be acquired in a separate transmission window. Significantly smaller crosstalk from ^{153}Gd should improve SNR and therefore would be expected to improve lymph node detection. We hypothesized that the use of a ^{153}Gd flood source would reduce background and improve SNR for these studies. **Methods:** Phantom studies simulating lymphoscintigraphy were performed to compare performance with a ^{153}Gd flood source, a ^{57}Co flood source, and no flood source. SNR in the ^{99m}Tc emission images was measured using a water phantom to simulate patient body and point sources of various activities to simulate nodes and injection site. The encouraging phantom studies prompted use of the ^{153}Gd flood source in routine clinical breast lymphoscintigraphy, melanoma lymphoscintigraphy, and lymphedema studies. Because emission and transmission data were acquired in separate energy windows, fused planar images of emission and transmission data were available to the physician. **Results:** SNR was highest with no flood source and was lowest with the ^{57}Co flood source by a significant margin. SNR with the ^{153}Gd flood source was similar to that with no flood source on the anterior (transmission) view. SNR was reduced somewhat in the posterior (nontransmission) view because of attenuation of signal by the flood source itself. Minor crosstalk in the ^{99m}Tc window was observed with the ^{153}Gd flood source, attributed to simultaneous detection of x-ray photons and gamma-photons. This crosstalk was reduced by introducing thin metal filters to absorb most x-ray photons, at the expense of more attenuation in the posterior view. Unlike with the ^{57}Co flood source, a usable posterior view (with anatomic shadow derived from the anterior view) was generated with the ^{153}Gd flood source. Clinical lymphoscintigraphy images with the ^{153}Gd flood source were of high quality. Interpretation was aided by the ability to control image mixing and brightness and contrast of separate color scales. **Conclusion:** By producing fused images with reduced crosstalk and improved image quality, a ^{153}Gd flood source offers advantages over a conventional ^{57}Co flood source for anatomic shadowing in lymphoscintigraphy. Lymph nodes in emission images have higher SNR, indicating a likely improvement in clinical lesion detection. Separate emission and transmission images provide additional flexibility in image display during interpretation.

Key Words: lymphoscintigraphy; ^{153}Gd; flood source; lymph node detection

J Nucl Med Technol 2015; 43:253–260

DOI: 10.2967/jnmt.115.161935

Unlike most nuclear medicine studies that image a radiopharmaceutical injected intravenously, scintigraphy of the lymphatic system involves intradermal or interstitial injection of the tracer, with localized imaging of the injection site and peripheral regions. For example, intradermal tracer injections about the site of a cutaneous melanoma are used to identify the sentinel lymph node (or nodes) receiving the lymphatic drainage from the primary tumor. In lymphedema studies of the lower extremities, tracer is injected into the dermis of the foot of the affected and unaffected limb. Rates of cephalad tracer migration are then used to assess for obstruction of lymphatic channels (*1*).

A disadvantage of lymphoscintigraphic studies is the absence of anatomic information in the images. This contrasts with nuclear studies using intravenous tracer administration, in which blood pool, organs, and other structures are often readily identifiable. In lymphoscintigraphy, there is virtually no systemic circulation of the tracer and such anatomy is not visible. This makes it difficult to correlate the findings on the scintigraphic images to anatomic landmarks identified in the operating room or on anatomic images.

One approach to provide anatomic localization of activity in lymphoscintigraphy is to acquire the images on a hybrid SPECT/CT scanner. However hybrid SPECT/CT imaging is not available in most laboratories. Moreover, the SPECT/CT acquisition requires longer imaging times and entails additional exposure to x-ray radiation. Effective

Received Jun. 12, 2015; revision accepted Jul. 31, 2015.

For correspondence or reprints contact: Frank P. DiFilippo, Department of Nuclear Medicine, Cleveland Clinic, 9500 Euclid Ave./Jb3, Cleveland, OH 44195.

E-mail: difilif@ccf.org

Published online Sep. 3, 2015.

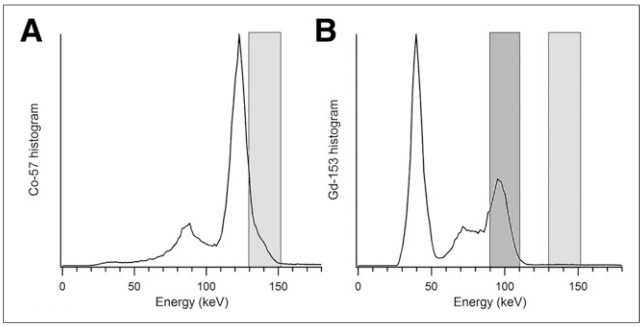

FIGURE 1. Energy spectra acquired for ^{57}Co flood source (A) and ^{153}Gd flood source (B). ^{99m}Tc emission window (140 keV, 15% width) is shown in light gray. With ^{57}Co flood source, many transmission photons are acquired in emission window, providing body outline in emission image but contributing crosstalk and reduced SNR. With ^{153}Gd flood source, transmission photons are acquired in separate window (100 keV, 20%) shown in dark gray. ^{153}Gd flood source contributes few counts to ^{99m}Tc emission window, arising from simultaneous detection of europium x-rays (40-keV peak) along with primary γ-photons (100-keV peak).

radiation dose from the CT scan is approximately 3 mSv, compared with less than 0.02 mSv for an external flood source (*2–4*). Planar scintigraphy is more practical and cost-effective for lymphoscintigraphy studies. A second approach to define anatomy is to inject ^{99m}Tc-pertechnetate intravenously in addition to the intradermal ^{99m}Tc-sulfur colloid injections. In a prior study, the detectability of sentinel lymph nodes was reported not to be affected by the ^{99m}Tc-pertechnetate counts (*5*). However, the higher background counts are expected to decrease the signal-to-noise ratio (SNR) and could prevent detection of less intense foci.

A common approach is to use an external ^{57}Co flood source to provide transmission data superimposed on the emission scintigraphy data (*1,6,7*). The flood source produces a clear outline of the body because most ^{57}Co photons in the body region are attenuated. The primary photons of interest emitted by ^{57}Co have energies of 122.1 keV (86% abundance) and 136.5 keV (11% abundance). Because the acquisition energy window for ^{99m}Tc is centered at 140.5 keV with a typical width of 15% (130–151 keV), most of the ^{57}Co 136.5-keV photons and some of the ^{57}Co 122.1-keV photons are detected in the ^{99m}Tc window (Fig. 1A). As a result, the image contains both the emission data from ^{99m}Tc and the transmission data from ^{57}Co.

To produce an anatomic shadow, the flood source must be placed facing the gamma-camera detector, on the opposite side of the body. For dual-detector cameras, a common technique is to tape the flood source to the opposite detector (with the detectors in 180° configuration, sometimes referred to as H-mode) to acquire the anterior view image with anatomic shadow produced by the flood source positioned posterior to the body. However, a disadvantage is that a simultaneous posterior view is not usable, because no anatomic shadow is produced, and because the ^{57}Co photons produce a high-count uniform background that dominates the ^{99m}Tc emission data. A workaround is to acquire sequential scans, 1 without and 1 with the ^{57}Co flood source in place, and to superimpose a mask on the posterior view based on a body outline derived from the anterior view with the flood source (*7*). This method, however, would double the scan time.

Reduced SNR in the ^{99m}Tc emission image is a concern when using a ^{57}Co flood source. Detecting low-activity foci of ^{99m}Tc-labeled sulfur colloid peripheral to the injection site is challenging if the background count density is high. Background counts arise from scattered photons from the intense injection site, from collimator penetration, and also from unattenuated photons from the ^{57}Co flood source. A low-activity ^{57}Co flood source is desirable to minimize background counts and thereby improve lymph node detection, but a high-activity ^{57}Co is desirable to produce a distinct body outline. Consequently, there is an optimal ^{57}Co activity and acquisition time that depends on lesion ^{99m}Tc activity, body habitus, and proximity to injection site, as well as the age of the ^{57}Co flood source (*4*).

An interesting alternative is to use a radionuclide such as ^{153}Gd to generate the anatomic shadow. The primary γ-photons emitted by ^{153}Gd have energies of 97.4 and 103.2 keV, with 29% and 21% abundance, respectively. These characteristics allow transmission photons to be acquired in a separate energy window (100 keV, 20% width) below that of the primary ^{99m}Tc emission window (Fig. 1B). Although there is downscatter from ^{99m}Tc into the transmission window, the emission data are virtually unaffected by the ^{153}Gd transmission sources. The advantages of ^{153}Gd as a transmission source were recognized in the 1980s (*8*). By the 1990s, ^{153}Gd line sources became available as an option on several SPECT imaging systems for transmission attenuation correction, intended mainly for cardiac imaging (*9*). With the development of hybrid SPECT/CT scanners, transmission attenuation correction is rarely available today. However, during that era, it was reported that a system using a scanning ^{153}Gd line source was useful for creating an anatomic shadow in lymphoscintigraphy scans (*10*). Compared with a ^{57}Co flood source, the ^{153}Gd transmission image was of much higher quality. Emission images were rescaled according to the intensity of sentinel nodes relative to the injection site and then were added to the transmission images to create final display images for interpretation.

We considered that an external ^{153}Gd flood source is a practical option for generating an anatomic shadow in lymphoscintigraphy scans. A ^{153}Gd flood source would be used in a manner similar to a ^{57}Co flood source, except that the emission and transmission data would be acquired in separate windows. Background counts in the emission window would be reduced, possibly improving SNR and lymph node detection. Images would then be interpreted using modern image fusion display software, with which anatomic and emission images are displayed in gray scale and in color, respectively, with variable intensity and mixing. We report on phantom studies and initial clinical experience using a ^{153}Gd flood source for anatomic shadowing.

MATERIALS AND METHODS

A custom ^{153}Gd flood source was purchased (FeatherLite; Eckert & Ziegler), with an activity of 270 MBq at the time of the phantom study (370 MBq at reference date) and 610 × 419 mm active dimensions. Phantom and clinical images were acquired with a dual-detector gamma-camera system (Symbia S; Siemens Molecular Imaging) with the detectors in 180° opposed configuration. Dual-energy windows were defined for the primary ^{99m}Tc emission data (140 keV, 15% width) and the ^{153}Gd transmission data (100 keV, 20%).

To assess imaging performance with a ^{153}Gd flood source relative to a ^{57}Co flood source, phantom studies were performed simulating lymph node detection in lymphoscintigraphy. A standard ^{57}Co flood source (C-Thru; Eckert & Ziegler) was available, with an activity of 177 MBq at the time of the phantom study (370 MBq at reference date) and 620 × 420 mm active dimensions. The geometry of the phantom studies is illustrated in Figure 2. A 20-cm cylinder filled with nonradioactive water was placed horizontally on the patient table and positioned between the 2 detectors. A flood source was placed above detector 2, underneath the table. Four point sources of ^{99m}Tc solution were prepared, with activities of 3,770, 800, 380, and 220 kBq and a maximum dimension 5 mm. The point sources were taped to the top of the phantom (facing detector 1), with the point source having the highest activity in the center and the 3 other point sources positioned 5 cm away, equidistant from each other in a triangular pattern. The highest activity point source represented an injection of ^{99m}Tc-sulfur colloid for a lymphoscintigraphy study, and the surrounding point sources represented downstream lymph nodes of lower activity. The ^{153}Gd or ^{57}Co flood source was positioned between the 2 detectors on top of the infrared sensor rails in front of detector 2, facing detector 1. The radial distance of each detector was adjusted such that the clearance between the phantom and detector 1 and the clearance between the table and detector 2 were each 10 cm.

One-minute static anterior and posterior images were acquired with separate energy windows (140 and 100 keV), as described above. A second set of images was acquired after rotating the phantom 180° to position the point sources on the bottom side of the phantom. Rotating the phantom allowed the point sources to be either attenuated or nonattenuated in the anterior and posterior views. Images were acquired with the ^{153}Gd flood source, ^{57}Co flood source, or no flood source in place above detector 2. Additional images were acquired using the ^{153}Gd flood source along with thin sheets of brass metal (thickness, 0.5 mm), 1 above and 1 below the source, to attenuate lower-energy photons (primarily europium x-rays) emitted during ^{153}Gd decay. Regions of interest were drawn on the 140-keV emission images, covering the extent of each point source to measure total lesion counts L, and regions of the same size were drawn nearby to measure background counts B. The SNR of each point source lesion was calculated:

$$\mathrm{SNR} = (\mathrm{L} - \mathrm{B})/\sqrt{\mathrm{B}}.$$

SNR was measured versus point source activity for anterior and posterior views and for all flood source configurations.

On the basis of the results of the phantom studies, our department began using the ^{153}Gd flood source in its clinical lymphoscintigraphy protocol, replacing the ^{57}Co flood source. The Cleveland Clinic Institutional Review Board approved the retrospective inclusion of representative clinical images in this article, and the requirement to obtain informed consent was waived. Breast and melanoma lymphoscintigraphy scans were acquired in standard views at 300 s per view with the ^{153}Gd flood source taped to the opposing detector. Whole-body lymphedema scans were acquired for both anterior and posterior projections, as the patient was scanned at 25 cm per minute in the axial direction with the ^{153}Gd flood source placed on the posterior detector. As with the phantom scans, the emission and transmission data were acquired in separate energy windows. In all these studies, the radiopharmaceutical was ^{99m}Tc-labeled filtered sulfur colloid as 4 injections of 3.7 MBq (100 μCi) per injection.

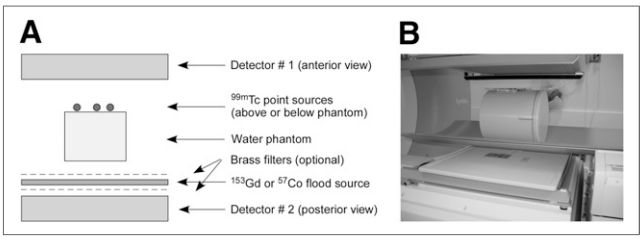

FIGURE 2. Schematic (A) and photograph (B) of phantom experiments simulating lymphoscintigraphy studies with flood source shadowing. In photograph, point sources are contained in 1-mL syringes taped to top of water-filled phantom. Images also were acquired with phantom rotated 180°, to position point sources on posterior side. Flood source (white) is visible in photograph (B), shown with 1 brass filter below source and none above source.

RESULTS

Representative phantom images are shown in Figure 3, for the case of anterior views with the point sources underneath the water-filled cylinder. With no flood source, all 4 point sources were visualized. With the ^{57}Co flood source, the shadow of the cylinder was visible in the ^{99m}Tc emission window. However, the additional background counts from the ^{57}Co flood source reduced image contrast, and the lowest-activity point source was not visualized clearly. With the ^{153}Gd flood source, no shadow of the cylinder was visible in the ^{99m}Tc window, and all 4 point sources were visualized with contrast similar to the case with no flood source. Similar visual image quality was obtained with the brass filters in place.

Lesion detection in the phantom studies was assessed quantitatively with SNR measurements. Figure 4 presents graphs of SNR versus point source activity for all flood source configurations and for all views. Views with point sources and the flood source on opposite sides of the cylinder (Figs. 4A and 4B) yielded lower SNR than unattenuated views with point sources and the flood source on the same side of the cylinder (Figs. 4C and 4D). The highest SNR was always obtained in the case with no flood source present, and the lowest SNR was always obtained in the case with the ^{57}Co flood source present. SNR with the ^{57}Co flood source was much lower in posterior views, in which the flood source illuminated the entire field of view and did not create a shadow. Compared with no flood source, SNR with the ^{153}Gd flood source and no brass filters was slightly lower

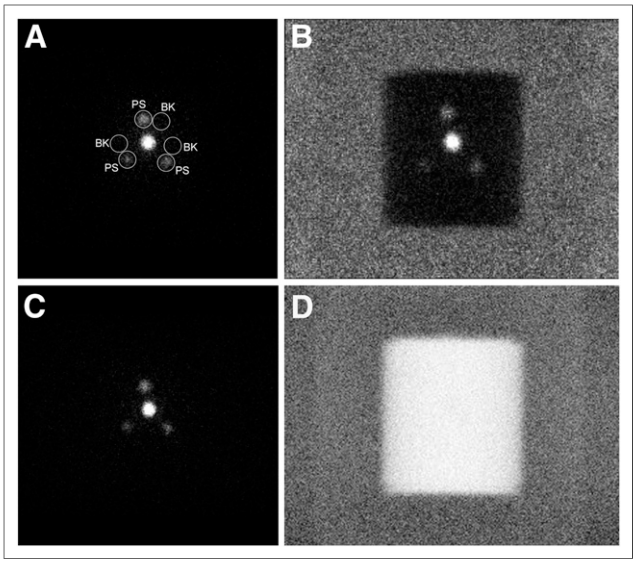

FIGURE 3. Anterior-view scintigraphy emission images (140-keV window) are shown in gray scale of water phantom with ^{99m}Tc point sources located below phantom: with no flood source (A), with ^{57}Co flood source (B), and with ^{153}Gd flood source (C). In A, circular regions of interest (diameter, 33 mm) for measuring point source counts (labeled PS) and adjacent background counts (labeled BK) are shown. For ^{153}Gd flood source, corresponding transmission image (100-keV window) (D) is shown in inverse gray scale. Point source activities were 3,770 kBq in center, 800 kBq at top, 380 kBq at lower-right, and 220 kBq at lower-left. All emission images are shown with equivalent intensity scaling relative to central point source.

in anterior views but was significantly lower in posterior views. The addition of the brass filters improved SNR in most cases to a small degree, but in 1 case (posterior view) the addition of brass filters degraded SNR slightly.

Clinical images were interpreted on a standard physician's workstation (Syngo MIApps; Siemens Molecular Imaging). On 1 screen, the ^{99m}Tc emission images were displayed alone in gray scale. On a separate screen, fused images were displayed with the ^{153}Gd transmission data in inverse gray scale and with the ^{99m}Tc emission data in color (Micro Delta hot metal color scale). The physician had full control over the brightness and contrast range and the percentage mixture of the gray scale and color scale images. For the posterior view of the whole-body images, the transmission image was generated from the anterior view transmission data, flipped horizontally to match the anatomy of the posterior view.

Examples of clinical lymphedema, breast lymphoscintigraphy, melanoma lymphoscintigraphy, and images are shown in Figures 5, 6, and 7. Lymphedema images were acquired as a whole-body scan with a 256 × 1,024 matrix and 25 cm/min table speed. Breast and melanoma lymphoscintigraphy images were acquired as 256 × 256 static views with 1.23 zoom at 300 s per view.

Region-of-interest measurements of the simulated phantom lesions were compared with lesions in the clinical studies. In the phantom images of Figure 3C, the background-subtracted region-of-interest measurements of the 3 peripheral point sources were 760, 430, and 250 counts. In the clinical images, the background-subtracted lesion counts were 110 counts for the inguinal node in Figure 5 (anterior view), 220 counts for the axillary node in Figure 6 (oblique view), and 360–560 counts for the 4 inguinal nodes in Figure 7 (anterior view).

DISCUSSION

An anatomic shadow in lymphoscintigraphy scans is useful to interpreting physicians. Lesions appear as isolated foci, often near the intense injection site, with virtually no anatomic information included in the ^{99m}Tc emission data itself. The ability to detect and localize lymph nodes in lymphoscintigraphy images may help guide surgery and affect treatment outcome.

Thus, a concern is whether the presence of the flood source has a significant negative impact on lymph node detection. With a ^{57}Co flood source, 1 approach is to acquire sequential scans with and without the source, producing a separate image unaffected by scatter and background counts from the ^{57}Co source for better lymph node detection. However, it is often not practical to acquire 2 sets of static views or whole-body views, which would add significant scan time, and most laboratories simply acquire 1 set of views with the ^{57}Co source. It has been demonstrated in phantom studies that there is an optimal ^{57}Co flood source activity and scan time for lymph node detection (*4*). The relationship is more complicated in clinical practice,

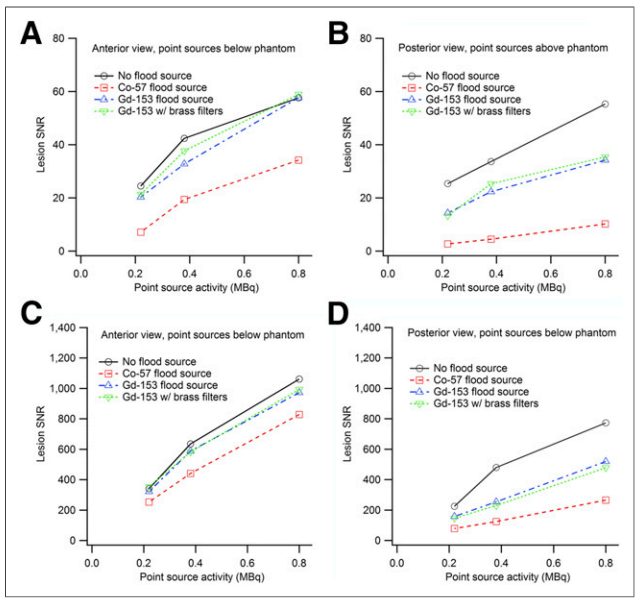

FIGURE 4. Graphs of SNR versus activity for 3 peripheral point sources in various phantom and flood configurations: anterior view, point sources below phantom (A); posterior view, point sources above phantom (B); anterior view, point sources above phantom (C); and posterior view, point sources below phantom (D).

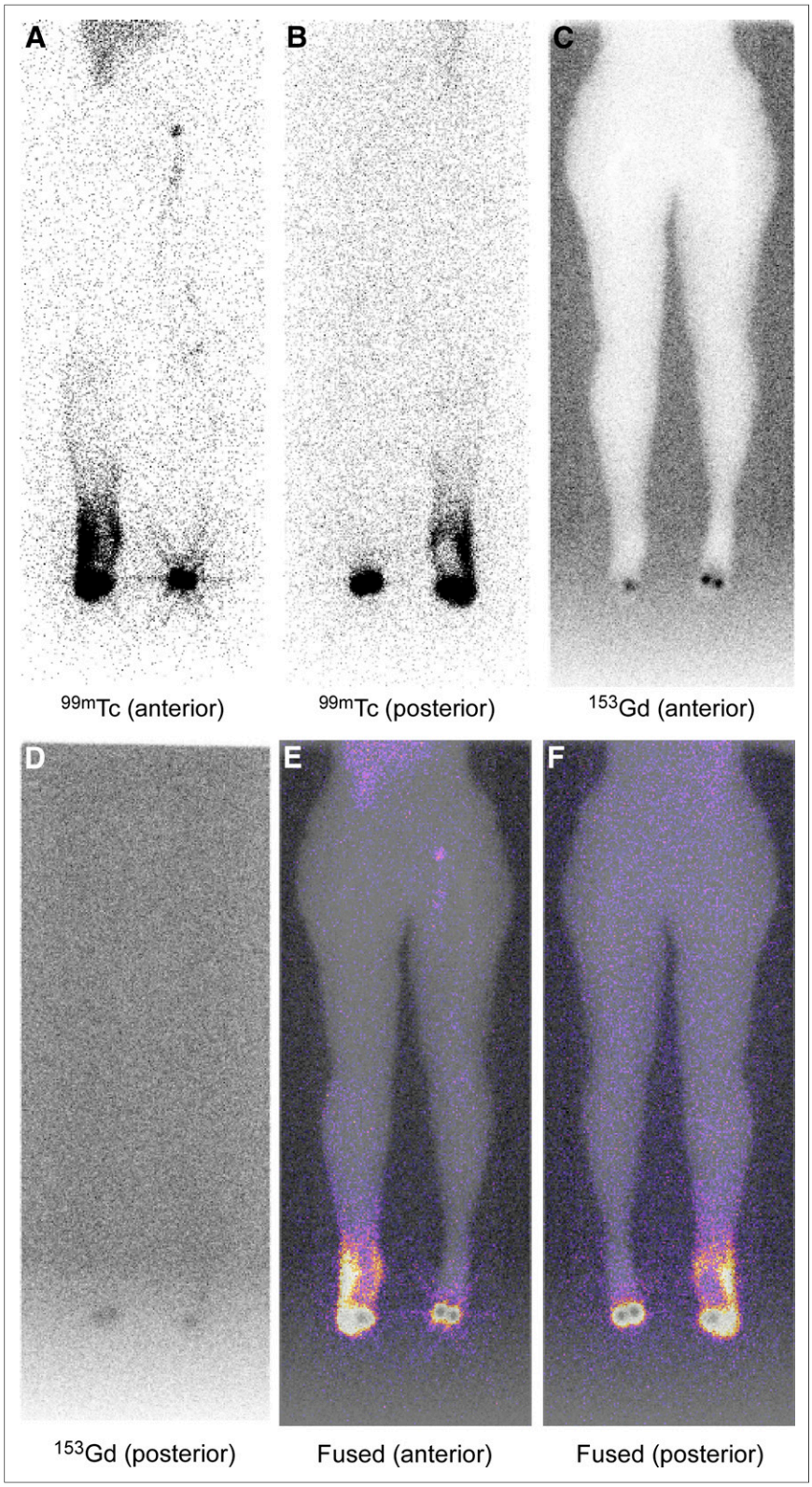

FIGURE 5. Example images from whole-body lymphedema scan: anterior and posterior views of ^{99m}Tc data, ^{153}Gd data, and fused ^{99m}Tc (color) and ^{153}Gd (inverse gray scale) data. Dermal backflow is clearly visible in ^{99m}Tc images, extent of which would not have been as apparent if ^{57}Co flood source had been used instead.

because parameters affecting lymph node detection include age (activity) of the decaying ^{57}Co flood source, lesion activity and size, injection site activity, proximity to the injection site, lesion depth, patient anatomy, camera energy resolution, collimator design, pixel size, and scan time. The fraction of clinical lesions that are missed due to the presence of the ^{57}Co source is unknown. However, the underlying rationale in clinical practice is that the benefit of an anatomic shadow with a ^{57}Co flood source outweighs the reduction in SNR.

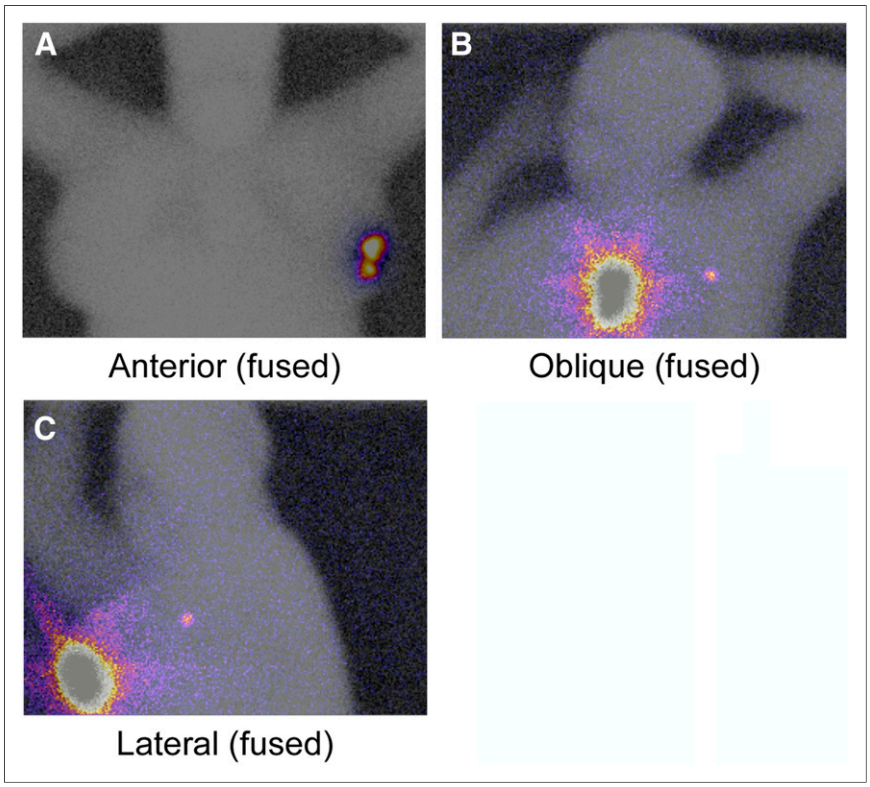

FIGURE 6. Example fused ^{99m}Tc (color) and ^{153}Gd (inverse gray scale) images from breast lymphoscintigraphy scan. ^{99m}Tc color window has been enhanced in oblique and lateral views to reveal lymph node with low tracer activity, which was not visible in anterior view and which would have had lower SNR if using ^{57}Co flood source and single energy window.

Replacing the ^{57}Co flood source with a ^{153}Gd flood source for lymphoscintigraphy scans is attractive for several reasons. The ^{153}Gd transmission photons in the 100-keV window do not interfere directly with the primary emission photons in the 140-keV window. Thus, there are fewer background counts with ^{153}Gd, compared with ^{57}Co, which improves SNR. With the ^{153}Gd source, the acquisition of emission and transmission counts in separate energy windows introduces flexibility in how images are displayed. The emission data can be displayed independently of the transmission data with a gray scale range that highlights the contrast of faint lesions that are difficult to detect. Fused emission and transmission images provide both functional and anatomic information in color and gray scale, respectively, which may aid interpretation and may provide better information to the referring physician or surgeon. The ^{153}Gd flood source also allows posterior views to be acquired simultaneously, by inverting the transmission image of the anterior view to create the posterior shadow. In whole-body lymphedema scans, for example, a posterior view may improve detection of popliteal nodes.

Another advantage of the ^{153}Gd flood source is that higher-quality anatomic shadows are generated. Given equal activity and scan time, an anatomic shadow from a ^{153}Gd flood source and 100-keV window has higher count density than a corresponding anatomic shadow from a ^{57}Co flood source and a 140-keV window, because only a small fraction of the primary ^{57}Co photons (122 keV) are acquired in the 140-keV window. Thus, a lower-activity ^{153}Gd source can produce anatomic shadows of acceptable quality, though further study is needed to determine the lowest acceptable activity for clinical use. The costs of a ^{153}Gd flood source and a ^{57}Co flood source are comparable, and the half-lives of ^{153}Gd (240 d) and ^{57}Co (272 d) are similar. Because the transmission data are acquired on-peak instead of off-peak, a ^{153}Gd flood source can be replaced less often than a ^{57}Co flood source for the purpose of anatomic shadowing. If

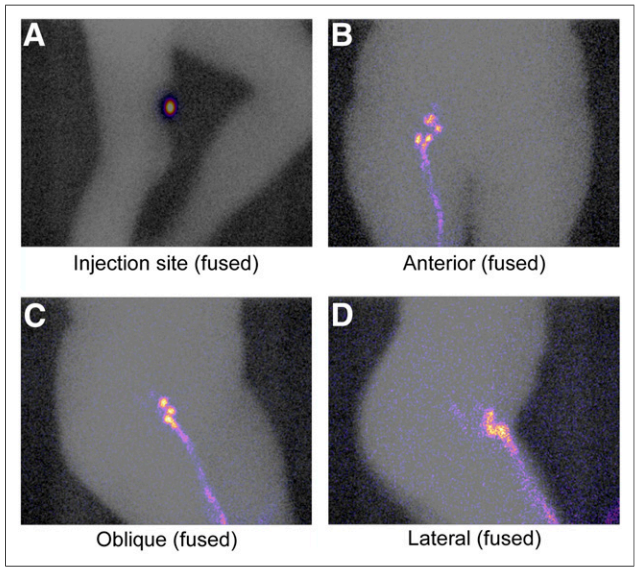

FIGURE 7. Example fused ^{99m}Tc (color) and ^{153}Gd (inverse gray scale) images from melanoma lymphoscintigraphy scan of injection site and of multiple views of inguinal lymph nodes.

a ^{153}Gd flood source can replace a ^{57}Co flood source for camera quality assurance and calibrations, then there is additional economic justification for replacing the ^{57}Co flood source entirely. However, equivalent performance between ^{153}Gd and ^{57}Co in quality assurance tasks must be validated for each specific camera model and supported by the manufacturer before replacing ^{57}Co with ^{153}Gd.

A minor issue with the ^{153}Gd flood source is the contribution to background counts from simultaneous detection of an approximately 100-keV γ-photon and an approximately 40-keV europium x-ray photon, which can produce a detected count in the 140-keV emission window. The added background counts from this mechanism are relatively small in the anterior view but may be noticeable in the posterior view. A thin layer of a suitable metal can be introduced to absorb preferentially the lower-energy x-rays and thereby reduce background counts. This effect was studied in the phantom experiments by adding brass filters to the ^{153}Gd source. A more ideal material would have been tin foil of approximately 0.15-mm thickness, but because inexpensive tin foil was not readily available, brass sheet metal of 0.5-mm thickness was used instead.

The phantom studies confirmed expectations of lesion detection versus the various configurations. SNR, which depends on the lesion counts and background counts, is influenced by many factors that are highly variable in clinical studies. Although the phantom studies encompassed a range of point source activities with or without attenuation and with or without flood sources, they did not represent the entire range of parameters encountered in clinical lymphoscintigraphy practice. Nonetheless, the phantom studies were valuable in comparing flood source configurations over a representative range.

As expected, imaging with no flood source produced the best SNR in all cases. This situation has minimal background counts, arising only from collimator penetration and scatter from ^{99m}Tc sources. The presence of a ^{57}Co or ^{153}Gd flood source only can reduce SNR, by contributing more background counts, by attenuating ^{99m}Tc photons (in the posterior view), or by contributing to detector dead time. SNR was reduced significantly in all cases with the ^{57}Co flood source. The degree of SNR reduction in the anterior view depended on signal strength (lesion activity and attenuation). In the posterior view where the ^{57}Co photons were unattenuated, the SNR was greatly reduced. The clinical implication is that some faint lesions in the anterior view may not be detected and that the posterior view most likely is not worth acquiring at all. The frequency of clinical lymph nodes missed when using a ^{57}Co flood source is an interesting topic for future research.

Replacing the ^{57}Co flood source with the ^{153}Gd flood source consistently improved SNR. Introducing brass sheet metal to filter x-ray photons further improved SNR in most cases. SNR in anterior views with the ^{153}Gd flood source and brass filters was similar to the case with no flood source present. This observation supports that the ^{99m}Tc emission data experience minimal interference from the ^{153}Gd source and that the interference arises from simultaneous detection of γ-rays and x-rays. In the posterior views, however, SNR with the ^{153}Gd flood source was substantially lower than the corresponding anterior views with the phantom rotated 180°. The reason for this difference is attenuation of ^{99m}Tc counts by the ^{153}Gd flood source. The presence of the brass filters further attenuated the ^{99m}Tc signal, though it also noticeably reduced background counts. Depending on whether the point sources were above or below the phantom, the presence of the brass filters either improved or reduced SNR in the posterior view. With point sources above the phantom and attenuated, background counts due to x-rays were a significant component in the posterior emission image, and SNR was improved by the brass filters. With point sources below the phantom and unattenuated, background counts due to x-rays were negligible, and the main effect of the brass filters was to attenuate signal, reducing posterior SNR.

The phantom studies provided confirmation of the superiority of the ^{153}Gd flood source compared with the ^{57}Co flood source for lymphoscintigraphy, and thus the ^{153}Gd flood source was adopted for use in clinical practice. Clinical lymphoscintigraphy images with ^{153}Gd shadow were of high quality, as can be seen from the examples in Figures 5–7. Figure 5 illustrates the utility of applying the ^{153}Gd flood source to a patient with lower-extremity lymphedema. Determination of the extent of dermal backflow is assisted by the availability of both anterior and posterior images and by the availability of emission-only ^{99m}Tc images, which avoid background counts arising from a ^{57}Co flood source. The potential benefit of an enhanced SNR with a ^{153}Gd flood source for anatomic localization is illustrated in the breast lymphoscintigraphy case in Figure 6, in which faint tracer uptake is identified in a sentinel lymph node in the anterior superior left axilla on oblique and lateral views. Finally, the images in Figure 7 clearly define the lymphatic pathway leading to the inguinal lymph nodes in a patient with cutaneous melanoma. The sentinel inguinal lymph nodes are clearly localized, and faint secondary iliac lymph nodes are visualized posterior to the inguinal nodes on the lateral view.

Further clinical studies will be needed to systematically evaluate the impact of the ^{153}Gd flood source in lymphoscintigraphy on clinical decision making. Initial reactions to the use of the ^{153}Gd flood source have been positive. Interpreting nuclear medicine physicians generally prefer the flexibility of emission-only and fused emission–transmission image display over their prior experience with a single image with ^{57}Co shadow. The brightness and contrast of the emission-only images are adjusted more easily without the border and background counts from the ^{57}Co source. Color screenshots of the fused emission–transmission images, in addition to gray-scale screenshots of the emission-only images, are routinely saved and made available to referring physicians and surgeons, facilitating the bedside

visualization of sentinel lymph nodes and pathways of lymphatic drainage.

CONCLUSION

A ^{153}Gd flood source offers several advantages over a ^{57}Co flood source for production of anatomic shadows in lymphoscintigraphy studies. The acquisition of emission and transmission data in separate energy windows yields both pure-emission and fused images and provides greater flexibility in image display. Phantom studies simulating lesion detection demonstrate superior SNRs using a ^{153}Gd flood source, which is attributed mainly to reduced background count levels compared with using a ^{57}Co flood source. The ^{153}Gd flood source is as practical to use in a clinical environment as a ^{57}Co flood source, having similar cost and radionuclide half-life. Lymphoscintigraphy with the ^{153}Gd flood source offers the potential for improved lymph node detection and improved satisfaction among referring physicians.

DISCLOSURE

No potential conflict of interest relevant to this article was reported.

REFERENCES

1. Giammarile F, Alazraki N, Aarsvold JN, et al. The EANM and SNMMI practice guideline for lymphoscintigraphy and sentinel node localization in breast cancer. *Eur J Nucl Med Mol Imaging.* 2013;40:1932–1947.
2. Law M, Ma WH, Leung R, et al. Evaluation of patient effective dose from sentinel lymph node lymphoscintigraphy in breast cancer: a phantom study with SPECT/CT and ICRP-103 recommendations. *Eur J Radiol.* 2012;81: e717–e720.
3. Krynyckyi BR, Sata S, Zolty I, Kim CK, Knesaurek K. Reducing exposure from ^{57}Co sources during breast lymphoscintigraphy by optimizing energy windows and other suggested enhancements of acquisition and the display of images. *J Nucl Med Technol.* 2004;32:198–205.
4. Mar MV, Dickinson RL, Erwin WD, Wendt RE III. Optimal ^{57}Co flood source activity and acquisition time for lymphoscintigraphy localization images. *J Nucl Med Technol.* 2008;36:82–87.
5. Wilczek B, Sandelin K, Eriksson S, Larsson SA, Jacobsson H. Sentinel node scintigraphy in breast cancer using a dual tracer technique. *Nucl Med Commun.* 2004;25:135–138.
6. Krynyckyi BR, Miner M, Ragonese JM, Firestone M, Kim CK, Machac J. Technical aspects of performing lymphoscintigraphy: optimization of methods used to obtain images. *Clin Nucl Med.* 2000;25:978–985.
7. Vallejo Mar M, Gee-Johnson S, Kim EE, Podoloff DA. Whole-body lymphoscintigraphy using transmission scans. *J Nucl Med Technol.* 2002;30:12–17.
8. Bailey DL, Hutton BF, Walker PJ. Improved SPECT using simultaneous emission and transmission tomography. *J Nucl Med.* 1987;28:844–851.
9. Zaidi H, Hasegawa B. Determination of the attenuation map in emission tomography. *J Nucl Med.* 2003;44:291–315.
10. Clarke E, Notghi A, Harding K. Improved body-outline imaging technique for localization of sentinel lymph nodes in breast surgery. *J Nucl Med.* 2002;43: 1181–1183.